Eleventh International Conference on CFD in the Minerals and Process Industries
CSIRO, Melbourne, Australia
7-9 December 2015

TRANSPORT AND DEPOSITION OF WELDING FUME AGGLOMERATES IN A REALISTIC HUMAN NASAL CAVITY

Lin TIAN[1], Kiao INTHAVONG[1], Göran LIDÉN[2], Yidan SHANG[1] , Jiyuan TU[1*] and Goodarz AHMADI[3]

[1]School of Aerospace, Mechanical and Manufacturing, RMIT University, Bundoora, VIC, AUSTRALIA
[2] Environmental Science and Analytical Chemistry, Stockholm University, Stockholm, SWEDEN
[3]Mechanical and Aeronautical Engineering, Clarkson University, Potsdam, NY, USA

*Corresponding author, E-mail address: jiyuan.tu@rmit.edu.au

ABSTRACT

Welding fume is a complex mixture containing ultra-fine particles in the nano-meter range. Rather than being in the form of a singular sphere, welding fume particles frequently agglomerate into long straight chains, branches or other forms of compact shapes. Understanding the transport and deposition of these nano-agglomerates in human respiratory systems are of great interest as welding fumes are a known health hazard. Accounting for various dynamic shape factors due to particle agglomeration, the current computational study is focused on the exposure route and the deposition pattern of the inhaled welding fume particles in a realistic human nasal cavity. For particles in the nano range, molecular diffusion is the dominant transport mechanism. Therefore Brownian diffusion, hydrodynamic drag, Saffman lift force and pressure gradient are included in the model study. The study shows that the human nasal cavity is most effective in capturing the inhaled agglomerates and the primary sphere size and the assembly form have significant influence to the deposition outcome.

NOMENCLATURE

A	particle projected area
c	surface sphericity
C_c	Cunningham correction
C_D	slip correction factor
d_A	surface equivalent sphere diameter
d_n	volume equivalent sphere diameter
F_B	Brownian diffusion force
F_D	hydrodynamic drag
g	gravitational constant
P_p	particle projected perimeter
Re	particle Reynolds number
t	time
u	slip velocity
ρ	fluid density
ρ_p	particle density
μ	fluid dynamic viscosity

INTRODUCTION

While in vivo measurements have identified the potential route of inhaled manganese particles to the basal ganglia of the brain via nasal olfactory deposition, details of such deposition in relation to the particle size, shape, airflow and the nasal airway morphology are generally unavailable (Fechter et al., 2002; Antonini et al. 2006; and among others). In complement to the in vivo experiment, computer simulation is frequently used to provide such information as it can track the inhaled particles in real time, allow localized particle motion analysis, and provide particle deposition statistics to characterize the transport process. Computational fluid dynamics (CFD) simulations have been widely used in the study of detailed flow pattern and particle transport characteristics in human respiratory systems. Among such effort, Katz and Martonen (1996), Zhang and Kleinstreuer (2001), Hofmann et al. (2003), Tian and Ahmadi (2012) employed computational models to investigate the airflow, and particle transport and deposition in the human tracheobronchial airways. Subramaniam et al. (1998), Matida et al. (2003), Kelly et al. (2004), Inthavong et al. (2006), and Zamankhan et al. (2006) applied the CFD methods in the human nasal/head airways for airflow and particle transport analysis. From various angles, these studies provide much detailed description of flow and particle features and allow wider coverage of flow and particle conditions, which would otherwise be difficult to infer from experimental measurements.

In this study, simulation of the transport and deposition of welding fume agglomerates in a realistic human respiratory airway, including the nasal cavity, larynx, trachea and first level of bronchia airway, was performed. Accounting for the various dynamic shape factors due to particle agglomeration, the current computational study is focused on the exposure route and the deposition pattern of the inhaled welding fume particles in the human nasal cavity. Particular attention is given to the deposition pattern and deposition rate of inhaled welding fume agglomerates, of manganese composition, in the nasal olfactory region, where subsequent diffusion to the basal ganglia of the human brain could occur.

MODEL DESCRIPTION

Welding Fume Agglomerates

Welding fume is a complex mixture containing fine particles of metal composition in nano scale. Rather than being in the form of a singular sphere, welding fume particles frequently agglomerate into long straight chains, branches or other forms of compact shapes. To simulate the welding fume agglomerates, long straight chains of 8, 20 60 spheres and compact agglomerates of 3 and 5

spheres are formed (Table 1). Primary spherical particle of 10 to 150 nm of partial manganese composition are considered in the assembly.

Diameter of Primary Spheres (nm)	*Welding Fume Agglomerates*
10 20 30 40 50 80 100 150	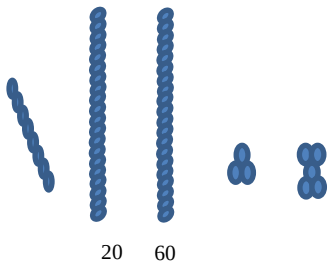

Table 1: Welding fume agglomerates in the computational study.

For spherical particles, the hydrodynamic drag F_D experienced is given as:

$$F_D = \frac{1}{2} C_D \rho U^2 A \quad (1)$$

where ρ is the fluid density, A is the projected area of the particle in the direction of the moving fluid , U is the slip velocity, and C_D is the slip correction factor. In the current study, empirical formulation of Tran et al. (2004) is used to describe the drag coefficient of the welding fume agglomerates. Rather than study on a limited number of solid shapes, the empirical equation of Tran et al. (2004) covers an infinite set of irregular shaped particles formed by an orderly arrangement of joined smaller spheres. In this formulation, C_D is given as:

$$C_D = \frac{24}{\mathrm{Re}} \frac{d_A}{d_n} \left[1 + \frac{0.15}{\sqrt{c}} \left(\frac{d_A}{d_n} \mathrm{Re} \right)^{0.687} \right] + \frac{0.42 \left(\frac{d_A}{d_n} \right)^2}{\sqrt{c} \left[1 + 4.25 \times 10^4 \left(\frac{d_A}{d_n} \mathrm{Re} \right)^{-1.16} \right]} \quad (2)$$

where d_A is the surface equivalent sphere diameter , d_n is the volume equivalent sphere diameter, and c is the surface sphericity given by $\pi d_A / P_p$, where P_p is the projected perimeter of the particle in its direction of motion, and *Re* is the particle Reynolds number given as:

$$\mathrm{Re} = \frac{\rho_p d_n U}{\mu} \quad (3)$$

here ρ_p is the particle density and μ is the fluid dynamic viscosity.

A computational fluid dynamics (CFD) model of the upper respiratory airway containing the nasal cavity, larynx, trachea and first bifurcation of the bronchial airway tree was developed from CT scans of individual regions of the human respiratory airway (Inthavong et al., 2009, 2010, 2011). Each model of the respiratory airway is connected to form a contiguous path from the nostril inlets to the upper tracheal region. Artificial straight tubes that extend from the first lung bifurcation were created to allow sufficient flow recovery and assist in numerical convergence of the CFD solution. The respiratory airway was added to a realistic human face exposed to the external surroundings containing airborne welding fume particles. A high quality mesh (minimum orthogonality > 0.1) incorporating prism layers was applied to the bounding respiratory walls. A tetrahedral unstructured mesh filled the airway passage. The mesh was gradually expanded out minimizing large changes in mesh size to resolve the fluid domain around the head. The final model is shown in Figure 1, which consists of 7 million cells. Grid consistency is tested and achieved.

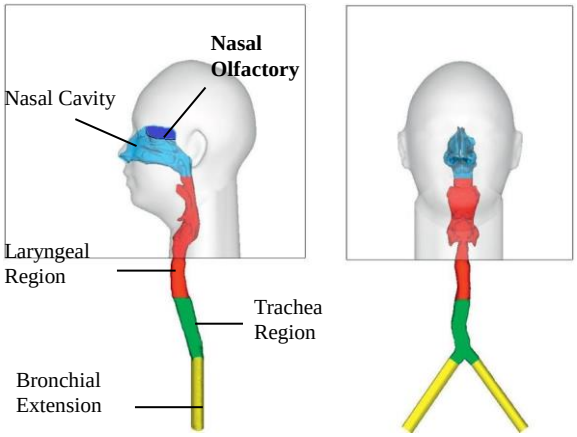

Figure 1: Human nasal and respiratory airway model.

Airflow Simulation

Assuming the cardiac load of welding operation is light to moderate, a steady laminar inhalation flow rate of 30 L/min was used. Based on the hydraulic diameter, the Reynolds number was 1050. The airflow field was simulated using the commercial CFD code, Ansys-Fluent v14.5. The surrounding walls were set to atmospheric pressure and inhalation is initiated by a negative pressure difference at the bronchial airway bifurcation relative to the ambient surroundings. This allows the flow field surrounding the face to be ambient and only influenced by the inhaled air. The continuity and momentum equation of the fluid flow are:

$$\frac{\partial}{\partial x_i} \left(\rho u_i \right) = 0 \quad (4)$$

$$\rho u_j \frac{\partial u_i}{\partial x_j} = -\frac{\partial p}{\partial x_i} + \frac{\partial}{\partial x_j} \left[\mu \frac{\partial u_i}{\partial x_j} \right] \quad (5)$$

here *u* and *p* are velocity and pressure of the air, *x* is the position in the coordinate. A second order upwind scheme is used to approximate the momentum equation, whereas the pressure-velocity coupling is handled through the SIMPLE method.

Particle Motion

Lagrangian particle tracking is used. An ensemble of 20,000 particles is released and each particle's trajectory is computed. The governing equation for particle motion is:

$$\frac{du_p}{dt} = \frac{1}{C_c} F_D + \frac{g(\rho_p - \rho_g)}{\rho_p} + F_B \qquad (6)$$

where u is the velocity, t is the time, g is the gravitational constant, ρ is the density, and subscripts p and g refer to the particle and gaseous phase respectively. F_D in Equation (6) is the drag force given by Equation (1) and (2), and C_c is the Cunningham correction. F_B is the Brownian diffusion force.

Model Validation

The particle equation in (6) is solved by stepwise integration over discrete time steps yielding a new particle velocity at each time step. In Ansys-Fluent, the length scale factor of integration controls the integration time step size. The integration time step Δt is then calculated by the specified length scale factor L_s, and the velocity of the particle (u_p) and of the continuous airflow phase (u_c):

$$\Delta t = \frac{L_s}{u_p + u_c} \qquad (7)$$

This means that the length scale factor is proportional to the integration time step, equivalent to the distance that the particle will travel before its equations are solved again and its trajectory updated. A smaller value for the length scale increases the number of calculations per distance length. Its selection must reproduce the diffusion dispersion mechanism for nanoparticles. A standard geometry in the form of a pipe (Figure 2a) with well-known solution by Ingham (1975) was used to validate the particle dispersion. Particle deposition in a pipe length of 0.9 m was compared for length scale factors of 5e-5 m, 1e-5 m, and 5e-6 m, which showed that the deposition was best described using a value of 1e-5 m

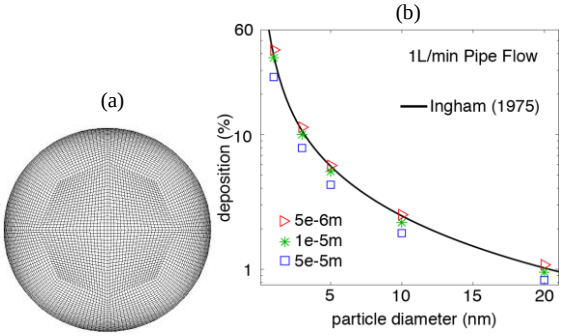

Figure 2: Model validation in a straight pipe: (a) pipe diameter = 0.0045 m, length = 0.09 m, mesh = 1,950,000 structured cells; (b) deposition efficiency.

RESULTS AND DISCUSSION

Assuming laminar flow, the stream wise airflow in the human nasal airway is given in Figure 3. High velocity magnitude is observed at the nostril, following by the nasal valve and the larynx. A small percentage (1.6%) of the inspiration air reaches the upper olfactory airway with significant lower velocity. Figure 4 displays the axial airflow velocity magnitude contours at selected cross sections along the mid-nasal airway.

Assuming a uniform concentration in human breathing zone, welding fume particles are released 5 cm in front of

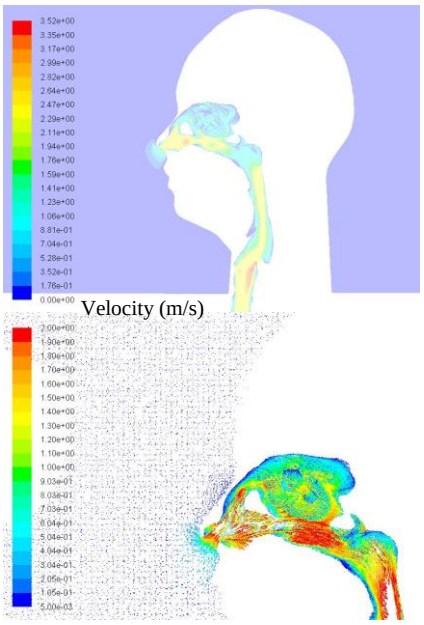

Figure 3: Stream wise airflow velocity contour and vector.

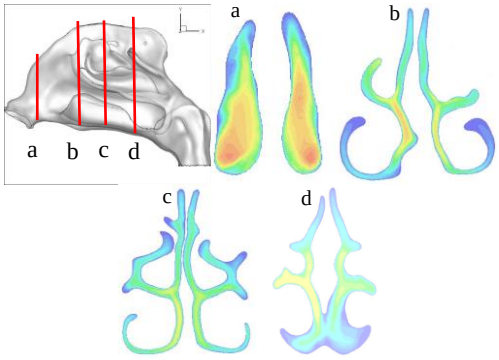

Figure 4: Axial velocity contours.

human face. Nasal trajectories of 6 selected sample particles are shown in Figure 5. Single sphere, compact agglomerates and agglomerates of shorter span (Figure 5a to 5d) are more likely to be dispersed into low velocity regions of superior and inferior meatus (Figure 4), while agglomerates of long straight chain (Figure 5e and 5f) are confined to reside in the bulk flow and follow the preferential pathway along the middle meatus toward the posterior nasal cavity (Figure 4). It is shown in Figure 5 that a very small fraction of the inhaled particles reach the nasal olfactory region (Figure 5b and 5d). Brownian diffusion is anticipated as the dominant driving force. Particle agglomerates of higher Brownian activity, such as single sphere, compact and short agglomerates are more likely to reach the nasal olfactory region.

Figure 6 displays the deposition efficiency of the inhaled particle agglomerates against the primary sphere size in the nasal cavity. By definition, deposition efficiency describes the ratio of the number of deposited particles to the total number of particles entering the nose via the nostril. From Figure 6, two regions can be identified. For particle and agglomerates with a primary sphere diameter larger than 50 nm, the deposition efficiency is low (< 3%). Variation of the deposition against primary sphere size is negligible. Variation of the deposition among different particle agglomerates is also less distinguishable. The

second region is for particle and agglomerates with the primary sphere diameter smaller than 50 nm. In this region, the deposition is highly sensitive to the form of the agglomeration and the size of the primary sphere. In general, high Brownian particles exhibits more deposition and for particle agglomerates with the least Brownian diffusion, minimum deposition is observed. In sequence of high to low, measured by the deposition efficiency, are the single sphere particle, 3-sphere compact agglomerates, 5-sphere compact agglomerates, 8-sphere chain agglomerate, 20-sphere chain agglomerate and the 60-sphere chain agglomerate. In this region, the deposition efficiency is in the range from 15% to 3% and varies monotonically with the primary particle size.

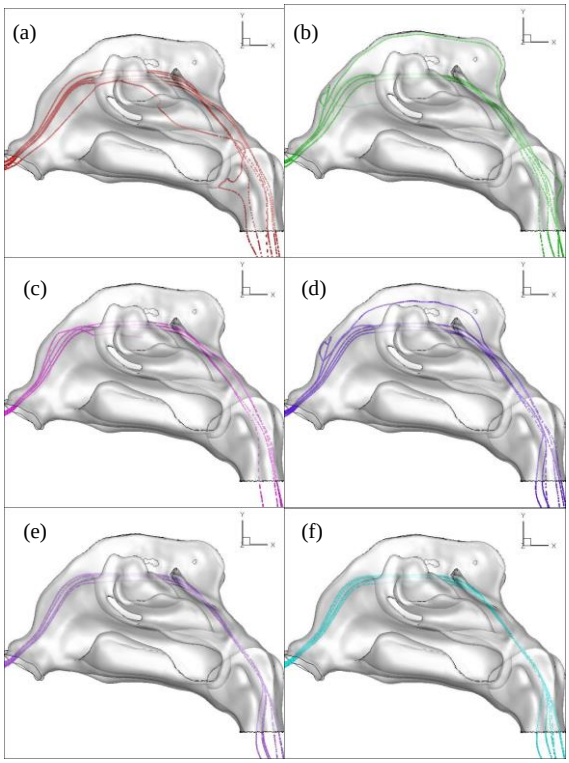

Figure 5: Particle trajectory in the nasal cavity with primary sphere of 20 nm: (a) single sphere; (b) 3-sphere compact agglomerates; (c) 5-sphere compact agglomerates; (d) 8-sphere chain; (e) 20-sphere chain; (f) 60-sphere chain.

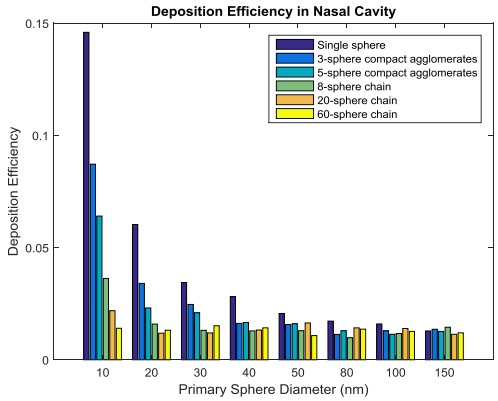

Figure 6: Particle deposition efficiency in the nasal cavity.

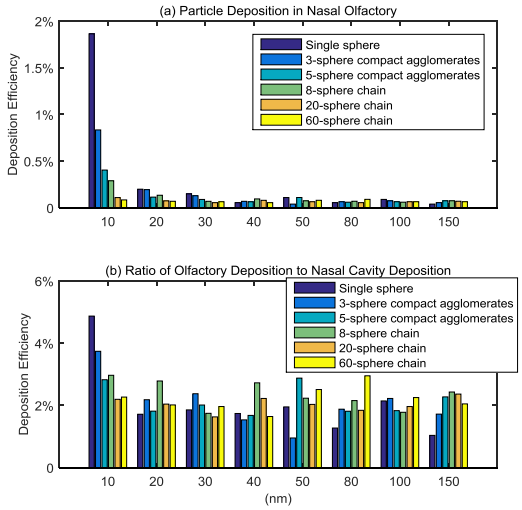

Figure 7: Nasal olfactory deposition pattern.

The nasal olfactory deposition pattern is displayed in Figure 7. Total deposition is the same as in Figure 6 where the ratio of the olfactory deposition number to the total number of particles entering the respiratory system is given. Regional deposition efficiency is defined as the ratio of the olfactory deposition to the number of particles deposited in the nasal cavity. It is shown in Figure 7.a that the overall total olfactory deposition is low, i.e., around 0.1% across all particle and agglomerates. The highest total olfactory deposition occurred for high Brownian diffusion particles of single spheres and compact agglomerates composed of 10 nm primary spheres (1.8% to 0.3%). As the size of the primary sphere increases, all particles and the agglomerates exhibit similar level of total deposition pattern in the nasal olfactory region. The regional deposition as shown in Figure 7.b indicates that as high as 12% of the nasal particle deposition could occur in the olfactory region for single sphere diameter of 10 nm, however for the majority of the particle and agglomerates, the relative deposition efficiency is around 4%.

CONCLUSIONS

The transport and deposition of welding fume agglomerates in human nasal respiratory airway are examined. The human nasal cavity is most effective in capturing the inhaled agglomerates. Deposition in the human nasal cavity occurred on anterior nasal septum and posterior nasal cavity near the nasopharynx. In the mid-nasal airway, the majority of the deposition occurred in the middle measus. A very small fraction of the inhaled welding fume agglomerates is dispersed into the nasal olfactory region and the deposition is extremely low. For nano-scale welding fume agglomerates, the primary sphere size and the assembly form have significant influence to the deposition outcome. Long straight chain agglomerates tend to be stabilized when following the main flow and less deposition occur. When primary sphere size reaches 50 nm, deposition variation with respect to primary sphere size and form of agglomerate is less distinctive.

REFERENCES

ANTONINI, J.M., SANTAMARIA, A.B., JENKINS, N.T., ALBINI, E., LUCCHINI, R., (2006), "Fate of manganese associated with the inhalation of welding fumes: Potential neurological effects", *NeuroToxicology*, **27**, 304-310.

FECHTER L.D., JOHNSON D.L. AND LYNCH R.A., (2002), " The relationship of particle size to olfactory nerve uptake of a non-soluble form of manganese into brain ", *NeuroToxicology*, **23**: 177-183.

HOFMANN, W., GOLSER, R. AND BALASHAZY, I., (2003), "Inspiratory deposition efficiency of ultrafine particles in a human airway bifurcation model", *Aerosol Science and Technology*, **37**, 988–994.

INGHAM, D.B., (1975), "Diffusion of aerosols from a stream flowing through a cylindrical tube". *Journal of Aerosol Science*, ***6***(2), 125-132.

INTHAVONG, K., TIAN, Z.F., LI, H.F., TU, J.Y., YANG, W., XUE, C.L. AND LI C.G., (2006), "A numerical study of spray particle deposition in a human nasal cavity", *Aerosol Science and Technology*, **40** (11), 1034-1045.

INTHAVONG, K., TU, J.Y., AND AHMADI, G., (2009), "Computational modelling of gas–particle flows with different particle morphology in the human nasal cavity", *Journal of Computational Multiphase Flows*, **1**(1), 57–82.

INTHAVONG, K., CHOI, L. T., TU, J. Y., DING, S., AND THIEN, F., (2010a), "Micron particle deposition in a tracheobronchial airway model under different breathing conditions", *Medical Engineering and Physics*, **32**(10), 1198–1212.

INTHAVONG, K., TU, J. Y., AND HESCHL, C. (2011), "Micron particle deposition in the nasal cavity using the v2-f model", *Computers and Fluids*, **51**(1), 184–188.

KATZ, I. AND MARTONEN, T.B. (1996), "Three-dimensional fluid particle trajectories in the human larynx and trachea", *J Aerosol Med*, **9(4)**:513-520.

KELLY, J.T., ASGHARIAN, B., KIMBELL, J.S. AND WONG B.A., (2004), "Particle deposition in human nasal airway replicas manufactured by different methods. Part I: Inertial regime particles", *Aerosol science and technology*, **38** (11), 1063-1071.

MATIDA, E. A., DEHAAN, W.H., FINLAY, W.H. AND LANGE, C.F., (2003), "Simulation of particle deposition in an idealized mouth with different small diameter inlets", *Aerosol Sci. & Tech.*, **37**, 924-932.

SUBRAMANIAM, R.P., RICHARDSON, R.B., MORGAN, K.T. AND KIMBELL, J.S., (1998), "Computational fluid dynamics simulations of inspiratory airflow in the human nose and nasaopharynx", *Inhalation Toxicology*, **10**, 91–120.

TIAN, L. AND AHMADI, G., (2012), "Transport and deposition of micron and nano particles in human tracheobronchial tree by an asymmetric multi-level bifurcation model", *Journal of Computational Multiphase Flow*, **4** (2), 159-182.

TRAN C.S., GAY, M, AND MICHAELIDES, E.E., (2004), "Drag coefficients of irregularly shaped particles", *Powder Technology*, **139**, 21– 32.

ZAMANKHAN, P., AHMADI, G., WANG, Z., HOPKE, P.H., CHENG,Y.S., SU, W.C. AND LEONARD, D., (2006), "Airflow and deposition of nanoparticles in a human nasal cavity", *Aerosol Science Technology*, **40**, 463-476.

ZHANG, Z. AND KLEINSTREUER, C., (2001), "Effect of particle inlet distributions on deposition in a triple bifurcation lung airway model", *Journal of Aerosol Medicine*, **14**, 13–29.

